ELSEVIER

Journal of Power Sources 93 (2001) 163–173

JOURNAL OF POWER SOURCES

www.elsevier.com/locate/jpowsour

Nickel hydroxide powder for NiO·OH/Ni(OH)$_2$ electrodes of the alkaline batteries

M.B.J.G. Freitas*

Universidade Federal do Espírito Santo, CCE, DQui, Grupo de Eletroquímica Aplicada, Av. Fernando Ferrari s/n, Goiabeiras, Vitória-ES, CEP:29060-900, Brazil

Received 3 August 2000; accepted 20 August 2000

Abstract

In the nickel hydroxide synthesis, the β-Ni(OH)$_2$ phase grows after total α-Ni(OH)$_2$ aging. A mixture of α-Ni(OH)$_2$ and β-Ni(OH)$_2$ phases is formed when a part of α-Ni(OH)$_2$ suffers aging. Galvanostatic oxidation of the α/β-Ni(OH)$_2$ produced by chemical synthesis formed a new type of active material. On discharge, it presented higher capacity than active material produced from β-Ni(OH)$_2$. Therefore, α/β-Ni(OH)$_2$ is a promising material for β-Ni(OH)$_2$ substitution, as a alternative precursor material used in the positive electrodes of alkaline batteries. Anions of the solution and water molecules are present in the nickel hydroxide powder. This is result of the synthesis method developed here. The characterization of the precursor material is determined with help of: X-ray diffraction, thermal analyses, Fourier transformation infrared spectroscopy, specific superficial area and electron scanning microscopy. © 2001 Elsevier Science B.V. All rights reserved.

Keywords: Nickel electrode; Alkaline batteries; Positive electrode

1. Introduction

There is great scientific and technological interest in the study of the nickel hydroxide synthesis, due to its application as positive electrodes of alkaline batteries. Nickel hydroxide can be formed as α-Ni(OH)$_2$ and β-Ni(OH)$_2$ phases. In the oxidation process β-NiO·OH or γ-NiO·OH phases can be obtained. In the α-Ni(OH)$_2$ lattice, the plane (0 0 1) is separated by intercalated water molecules and alkali metal ions. The lattice parameters for unit cell in the hexagonal system are $c_0 = 8.05$ Å and $a_0 = 3.08$ Å. α-Ni(OH)$_2$ is unstable in the presence of alkali, and by aging, that is, with water and alkali metal ions elimination it becomes β-Ni(OH)$_2$ [1–3]. Due to α-Ni(OH)$_2$ instability in alkaline solutions, β-Ni(OH)$_2$ is frequently used as a precursor material in alkaline batteries [4]. Lattice parameters for β-Ni(OH)$_2$ in the hexagonal system are $c_0 = 4.65$ Å and $a_0 = 3.12$ Å [1]. In the β-NiO·OH phase, the hexagonal structure of the β-Ni(OH)$_2$ is maintained. Furthermore, mass reduction and contraction of the lattice volume [5–7] occurs. The lattice parameters in the hexagonal system are $c_0 = 4.84$ Å and $a_0 = 2.81$ Å. γ-NiO·OH which represents a family of chemical compositions that has as a general formula $A_xH_y(H_2O)NiO_2$ (x, $y \leq 1$), where A represents alkaline metals specially Na^+ and K^+. It has water molecules intercalated between the (0 0 1) planes. The lattice parameters in the hexagonal system are $c_0 = 7.2$ Å, $a_0 = 2.82$ Å [1–3]. γ-NiOOH is obtained from β-Ni(OH)$_2$ unless the following conditions: long time of load, alkali high concentrations and imperfections in the crystals [4]. Trying to improve the behavior of the NiO·OH/Ni(OH)$_2$ electrodes, has involved several modifications to the nickel hydroxide microstructure [8–9]. In this work, a study of the relationship between nickel hydroxide microstructure and the performance of the NiO·OH/Ni(OH)$_2$ electrodes was carried out. The materials were characterized in different stages of preparation with help from the following techniques: X-ray diffraction, Fourier transform infrared spectroscopy (FT-IR), thermodifferential (TDA) and thermogravimetric analyses (TGA) and specific superficial area (BET) and electron scanning microscopy.

2. Experimental

The chemical synthesis was made in three stages: (1) addition of the reagents; (2) digestion of the precipitate; (3) drying and grinding of the precipitate. In the third stage, the precipitate was dried under such conditions that water was

* Tel.: +55-21-27-3352486; fax: +55-27-3352460.
E-mail address: marcosbj@hotmail.com (M.B.J.G. Freitas).

0378-7753/01/$ – see front matter © 2001 Elsevier Science B.V. All rights reserved.
PII: S0378-7753(00)00570-X

not totally eliminated. This could cause a decrease in the electrochemistry activity of the nickel hydroxide, as initially found by Micka and Zabransky [10]. In the grinding of the agglomerates, the nickel hydroxide powder obtained was ready to be used in sintered, pasted, tubular or pressed positive electrodes of the alkaline battery.

2.1. Synthesis A

The synthesis A was made as follows: one solution of the NH_4OH 1.0 mol/l was added by dripping in the $Ni(NO_3)_2$ 1.0 mol/l solution at the rate of 10.0 ml/min. During the base addition, the suspension was in constant stirring. The addition of NH_4OH 1.0 mol/l solution stopped when the pH was equal to 10. When the addition of the reagent was done, the digestion process began and lasted for 24 h. After this, the precipitate was washed in order to remove the excess of NH_4^+, NO_3^- and OH^- ions. Due to great solubility of the nitrate, it was impossible to do any visual test to observe the end of the washing process. Therefore, the precipitate was washed five times. In each precipitate wash, the separation between the solution and the solid was done by centrifugation at 1500 rpm for 50 min. In the next stage, the precipitate was dried at 50°C for 72 h. The nickel hydroxide mass remained constant in these conditions. The precipitate was then pulverized and the powder past through a 37 mesh opening sieve.

2.2. Synthesis B

In the synthesis B, KOH and $NiSO_4$ were used as reagents. One solution of KOH 1.0 mol/l was added by dripping at a speed of 10 ml/min on to $NiSO_4$ 1.0 mol/l solution maintaining in constant stirring. The reagent addition was concluded when the pH of the suspension reached 13. In the next stage, the precipitated digestion began and lasted 24 h. Soon after, the precipitated wash happened, which led to the removal of the excess reagent. The separation between the precipitate and the solution was done by centrifugation at 1500 rpm for 50 min. After the sedimentation of the precipitate, an aliquot was removed of the upper solution. $BaCl_2$ 1.0 mol/l in excess was added to the solution, causing precipitation of $BaSO_4$. The wash of the precipitate was concluded when the white precipitate of $BaSO_4$ was no more found in the wash water. This approach was adopted to conclude the wash operation. This lowered on average, after five washes of the precipitate. The nickel hydroxide was dried at 50°C for 72 h. After this drying time, the mass of nickel hydroxide remained constant. Finally the precipitate was pulverized and passed through a 37 mesh opening sieve.

2.3. Electrochemical cell

The working electrode was prepared by pasting and thermopressing of the nickel hydroxide paste under a grid of carbon steel. Additives used were graphite and low-density polyethylene (LDPE). The powder weight was optimized at 52 wt.% nickel hydroxide, 21 wt.% graphite and 27 wt.% LDPE. The graphite powder and LDPE had spherical diameter of 15 and 500 μm, respectively. The pasted electrodes were prepared applying a paste in the grid. The paste optimization was done measuring its density as a function of the water weight. The plasticity region was reached when about 25 wt.% of water in the total paste weight is obtained. The pasted electrodes were dried for 3 h at room temperature and 60% of air humidity. Then, the water came out, leaving pores in the paste. Afterwards, the electrodes were thermopressed in the following optimized conditions: 140°C, 840 kg/cm^2 for 7 min. After thermopressing, the positive plates had 1.0 mm of thickness and 3.2 cm^{2}of area (in the both sides of the electrodes). The current density for formation (i_f), discharge (i_d) and charge (i_c), were equal to 0.5 mA/cm^2 or 23.0 mA/g (the current divided by nickel hydroxide mass). In the wetting process, before galvanostatic formation, the electrodes were immersed in a solution of KOH 5.0 mol/l and LiOH 1.0 mol/l for 24 h. The electrochemical measurements were accomplished in LDPE cells with capacity for 100 cm^3 of KOH 5.0 mol/l and LiOH 1.0 mol/l work solution. The auxiliaries electrodes were two nickel plates with 3.5 cm^2 of superficial area and 0.1 mm of thickness. To homogenize the electric field, the work electrode was placed between the auxiliaries electrodes. The distance between the work electrode and the auxiliaries was on average 2.0 cm. A Hg/HgO in the same work solution was used as reference electrode. The chemical solutions were prepared with reagent grade quality. Distillated water was boiled to eliminate the presence of CO_2. This was done to avoid the carbonate formation in alkaline solution. Galvanostatic experiments were made with the help of a regulated power supply Fac-model 200 coupled with a timer built in the laboratory. The potential recording was the ECB model RB 101. The specific capacity obtained in galvanostatic discharge was expressed in mAh/g (capacity per mass of the initial nickel hydroxide powder).

2.4. Characterization techniques

The following techniques were used for material characterization: X-ray diffraction, Fourier transformation infrared spectroscopy, thermodifferential and thermogravimetric analyses, superficial area (BET) and electron scanning microscopy. The measurements were carried out by using the following instruments: Rotaflex-Rigaku model 200B diffractometer, Bomem model 102 spectrophotometer, thermal meter Netzsch STA 409, meter ASAP-2000 V-2.04 and Zeiss model DSM 940 interfaced to microcomputer IBM-PC. The centrifugation of the nickel hydroxide precipitated was done with a centrifugal Fek Brake model Top M03.

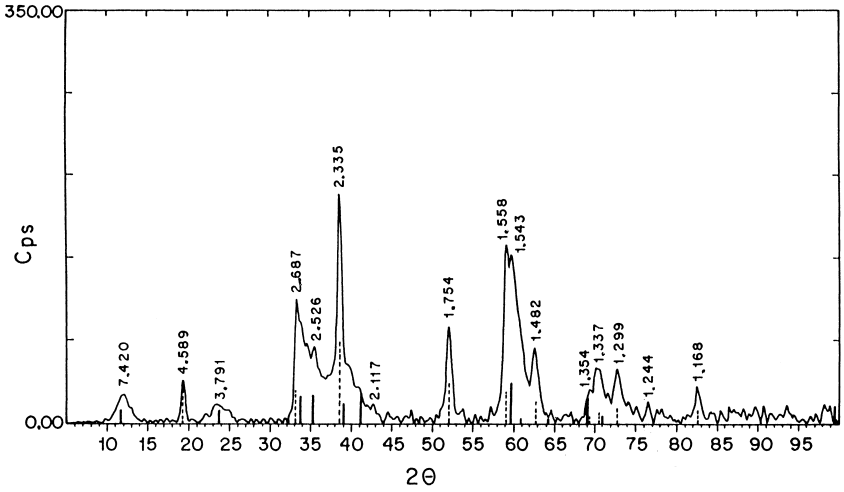

Fig. 1. X-ray diffraction pattern for nickel hydroxide synthesized for the method A, full line for alpha-nickel hydroxide, dotted line for beta-nickel hydroxide.

3. Results and discussion

3.1. X-ray diffraction

A typical example of X-ray diffraction for nickel hydroxide synthesized for the method A is shown in the Fig. 1. In this figure, the interlayer distances (d) can be seen close to the diffraction peaks, to simplify its identification. In comparison with JCPDS cards [11,12], it was verified that the nickel hydroxide was formed by a mixture of the alpha and beta phases. It demonstrates that α-$Ni(OH)_2$ did not totally become in β-$Ni(OH)_2$ in the aging process. The diffraction peaks enlargement was due to the small size of crystallites. The mean thickness of the crystallites, normal to (0 0 1) diffraction plane ($2\theta = 11.8°$), was calculated with Scherrer's equation and the value found was 400 Å. Overposition peaks of α-$Ni(OH)_2$ and β-$Ni(OH)_2$ also contributed to enlargement. The α-$Ni(OH)_2$ amount found in the α/β-$Ni(OH)_2$ mixture was determined by intensity integration of the (0 0 1) peaks for α-$Ni(OH)_2$ and β-$Ni(OH)_2$. The result was equal to 60%.

A typical example of X-ray diffraction for nickel hydroxide synthesized for the method B is shown in the Fig. 2.

The interlayer distance (d) and the relative intensities (I/I_0) were in full agreement with those corresponding to β-$Ni(OH)_2$ [12]. The peak enlargement can be attributed to small crystallite size. Its thickness calculated by using Scherrer's equation and normal to (0 0 1) diffraction plane ($2\theta = 19.3°$) is equal to 305 Å. Then, X-ray measure showed that very small crystallites formed the alpha/beta nickel hydroxide and beta nickel hydroxide powders. This was a consequence of the laboratory method developed for precursor material synthesis.

3.2. Fourier transformation infrared spectroscopy

FT-IR absorption spectra for alpha/beta nickel hydroxide was made to complement the X-ray measures (Fig. 3). The

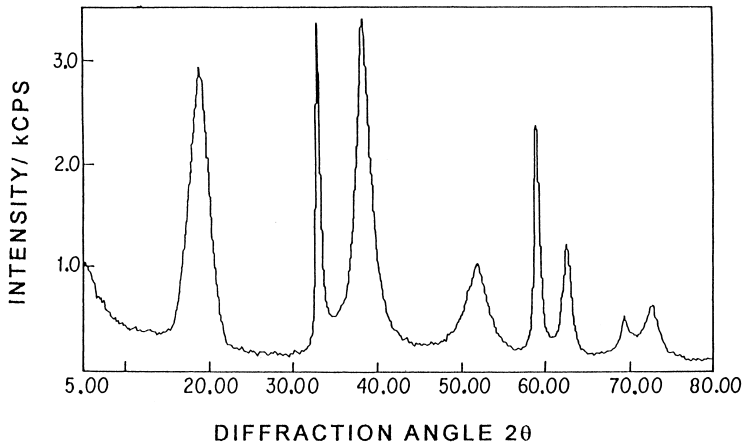

Fig. 2. X-ray diffraction pattern for nickel hydroxide sinthesized for the method B, beta nickel hydroxide.

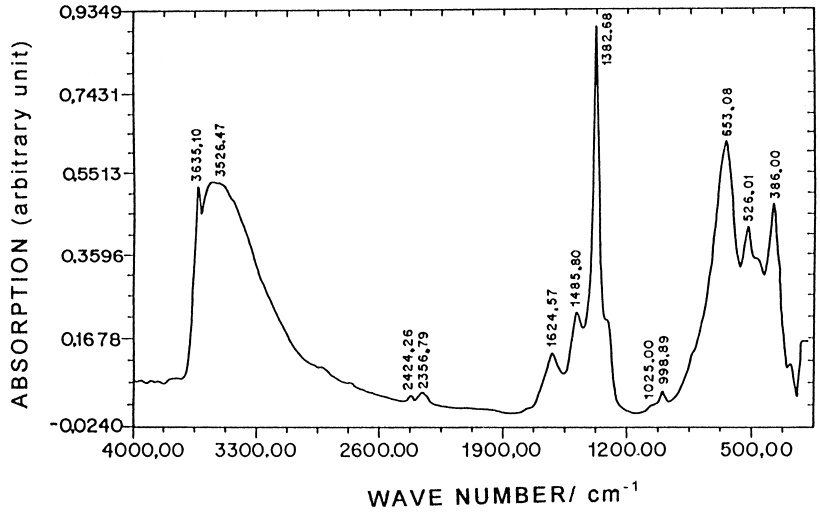

Fig. 3. Infrared absorption spectra for alpha/beta nickel hydroxide.

FT-IR spectra shows that, the alpha/beta nickel hydroxide powder retains nitrate and carbonate anions proceeding from the mother solution. The presence of carbonate is due to the open system used in the synthesis. FT-IR spectra also has characteristic bands of water molecules. The absorptions bands follow the attributions below [2,13]:

3635 cm^{-1}	vibrational stretching of hydroxyl group in the nickel hydroxide lattice
3526 cm^{-1}	vibrational stretching of hydroxyl group of the intercalated and adsorbed water
2424 and 2356 cm^{-1}	CO_2 present in the air
1624 cm^{-1}	water angular deformation
1485 cm^{-1}	nitrate anion
1382 cm^{-1}	carbonate and nitrate anions
1025 cm^{-1}	(shoulder) carbonate anion
998 cm^{-1}	nitrate anion
653 cm^{-1}	Ni–N vibrational stretching
526 cm^{-1}	water angular deformation in plane
457 cm^{-1}	(shoulder) Ni–O vibrational stretching
386 cm^{-1}	water angular deformation outside-of-plane.

A typical example of FT-IR spectra for beta nickel hydroxide is shown in the Fig. 4. It presents characteristic bands for sulfate, carbonate and adsorbed water. The absorptions bands follow the attributions below [2,13]:

3637 cm^{-1}	vibrational stretching of hydroxyl group in the nickel hydroxide lattice

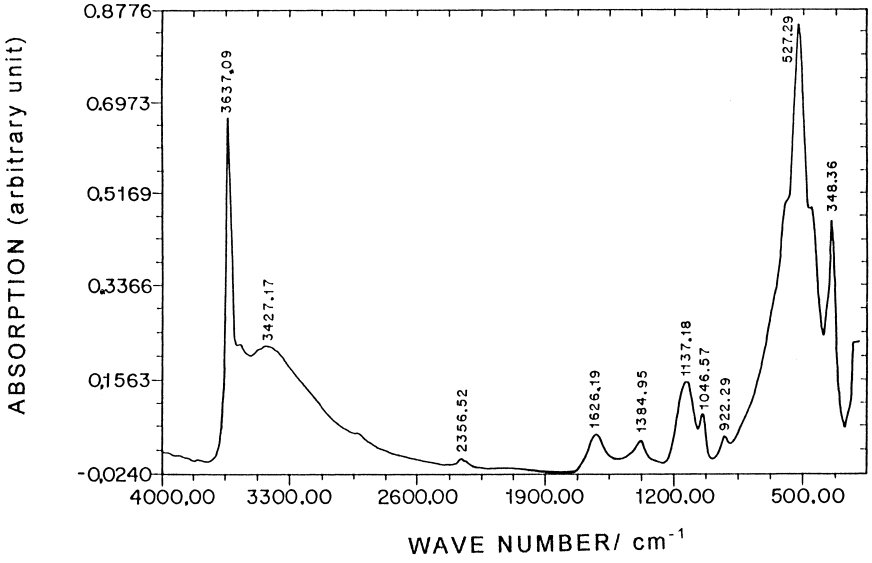

Fig. 4. Infrared absorption spectra for beta nickel hydroxide.

3427 cm^{-1}	stretching vibrational of hydroxyl group of the adsorbed water
2356 cm^{-1}	CO_2 present in the air
1626 cm^{-1}	water angular deformation
1384 and 1046 cm^{-1}	carbonate anion vibration stretching
1137 and 922 cm^{-1}	sulfate anion
527 cm^{-1}	water angular deformation in plane
457 cm^{-1}	Ni–O vibrational stretching
348 cm^{-1}	water angular deformation outside-of-plane.

3.3. Thermogravimetric analysis

Fig. 5 shows a typical thermogravimetric plot for α/β-$Ni(OH)_2$. The percentage of relative mass loss is plotted against the temperature increase. There are two temperature intervals where significant mass loss can be detected. The first one is the interval between 40 and 200°C that corresponds to elimination of adsorption and intercalation water. The second is the range between 200 and 450°C that corresponds to reaction: $Ni(OH)_2 \rightarrow NiO + H_2O$ and the desorptions of nitrate and carbonate anions [14,15]. NiO calcination occurred in the temperature range between 450 to 700°C, before the beginning of the powder sintering. Quantitative analysis was made with previous knowledge of the following data: the initial values of nickel hydroxide mass (22.9 mg) and the relative water loss in the interval between 40 and 200°C (11.2 wt.%). The fraction between the amount of substance (mol) of water and α/β-$Ni(OH)_2$ was 0.64. This characterization does not supply the relative contribution for intercalated and adsorbed water. The water intercalated in the α/β-$Ni(OH)_2$ caused (0 0 1) interlayer expansion. This can be confirmed in the diffraction patterns shown in Fig. 1, where (0 0 1) interlayer distance increases from 4.6 ($2\theta = 19.2°$) to 7.4 Å ($2\theta = 11.8°$) due to water intercalation. Chemical composition for alpha/beta nickel hydroxide is in agreement with thermogravimetric, X-ray diffraction and infrared spectroscopy measurements can be expressed as follows:

$$\left[\alpha/\beta\text{-}Ni(OH)_{2\text{-}K}(H_2O)_{0,65}(NO_3)_{2\text{-}U}(CO_3)_{2\text{-}W}\right],$$

where 2-K, 2-U and 2-W are the amounts of substances (mol) for OH^-, NO_3^- and CO_3^{2-}, respectively.

In the thermogravimetric plot of beta nickel hydroxide (Fig. 6 is a typical example) there are two temperature intervals with significant mass loss. In the first interval, between 40 and 200°C, the mass loss is attributed to the elimination of adsorbed water.

The quantitative analysis of beta nickel hydroxide is done with previous knowledge of initial mass (131 mg) and the relative mass loss (5.7 wt.%) of nickel hydroxide, in the interval between 40 and 200°C. The fraction between the amount of substance of water and beta nickel hydroxide is equal to 0.30. The reduction in the amount of water is due to experimental procedure. It is in agreement with the X-ray diffraction spectra that does not show expansion of the interlayer distance in beta nickel hydroxide lattice (Fig. 2). The second interval with significant mass loss is between 200 and 450°C and corresponds to the reaction: $Ni(OH)_2 \rightarrow NiO + H_2O$ and sulfate and carbonate anions desorptions. From 450 to 700°C, the NiO calcination process occurred. Chemical composition for beta nickel hydroxide can be written as follows:

$$[\beta\text{-}Ni(OH)_{2\text{-}X}(H_2O)_{0,30}(SO_4)_{2\text{-}Y}(CO_3)_{2\text{-}Z}],$$

where 2-X, 2-Y and 2-Z are the amounts of substances for OH^-, SO_4^{2-} and CO_3^{2-}, respectively.

3.4. Thermodifferential analysis

In the thermodifferential plot for alpha/beta and beta nickel hydroxide two endothermic peaks could be seen (Figs. 7 and 8).

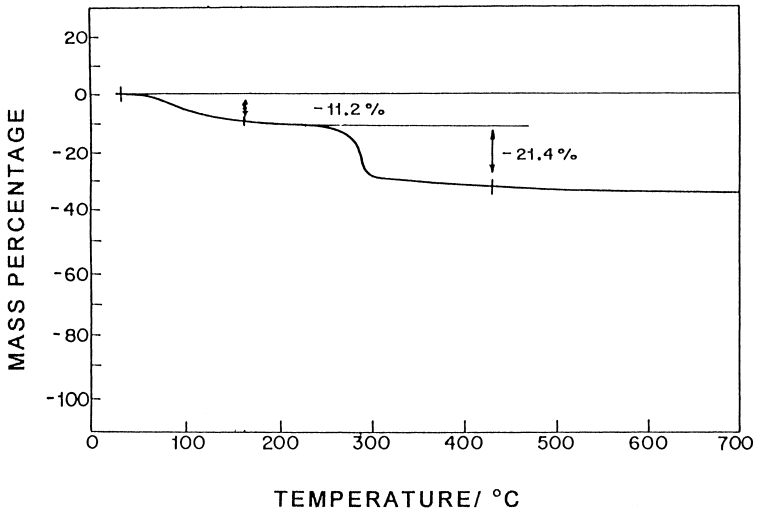

Fig. 5. Thermogravimetric plot for alpha/beta nickel hydroxide, temperature scan of the 7°C per minute, initial mass = 22.9 mg.

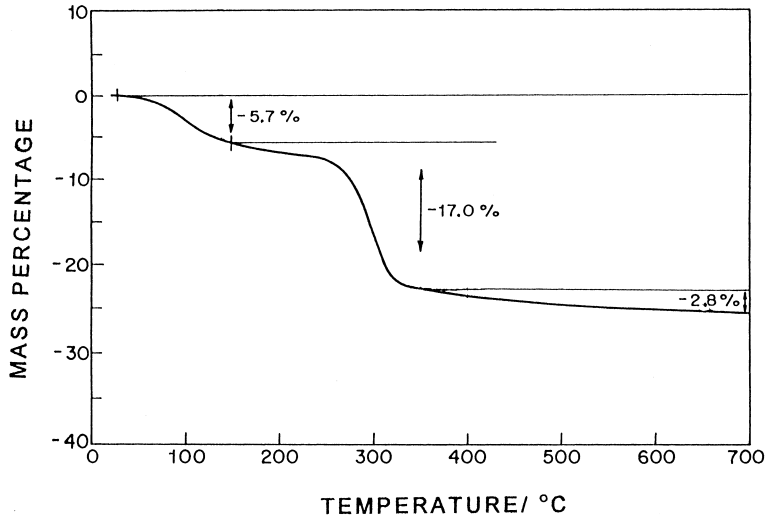

Fig. 6. Thermogravimetric plot for beta nickel hydroxide, temperature scan of the 7°C per minute, initial mass = 131 mg.

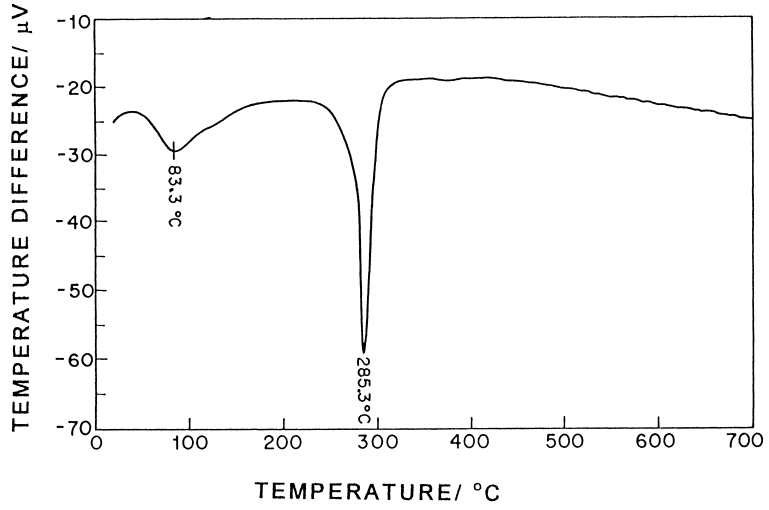

Fig. 7. Thermodifferential plot for alpha/beta nickel hydroxide, temperature scan of the 7°C per minute, initial mass = 22.9 mg.

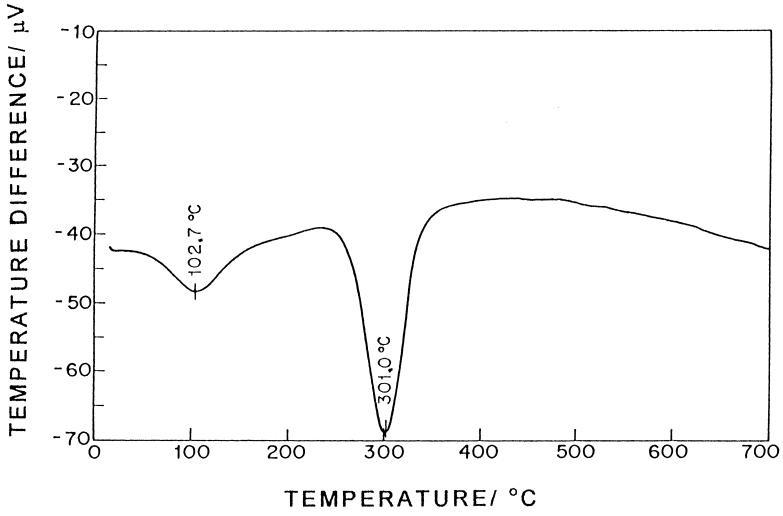

Fig. 8. Thermodifferential plot for beta nickel hydroxide, temperature scan of the 7°C per minute, initial mass = 131 mg.

Table 1
Specific surface area

Material	BET (m^2g^{-1})
Alpha/beta nickel hydroxide	35
Beta nickel hydroxide	114

The first response in the temperature interval between 40 and 200°C is due to elimination of the water of adsorption and intercalation for alpha/beta nickel hydroxide and water of adsorption for beta nickel hydroxide [15]. The second occurs at a temperature interval between 200–450°C corresponding to the $Ni(OH)_2$ decomposition and loss of anions of the mother solutions presented in the nickel hydroxide powder. The thermodifferential plot is in total agreement with thermogravimetric one.

3.5. Specific superficial area

As shown in the Table 1, the alpha/beta nickel hydroxide has BET superficial area smaller than the one of beta nickel hydroxide. It is due to the largest amount of water present in the alpha/beta nickel hydroxide that forms chemical bonding between the crystals resulting in a more agglomerated powder.

3.6. Electrochemical characterization of the active material

3.6.1. Active material formation

A typical chronopotentiogram of the formation process at the same current density, can be seen in Fig. 9 for alpha/beta nickel hydroxide and beta nickel hydroxide. In general, in the formation process, there is an overpotential peak, due to the growth of the first nuclei of the active material. With the nuclei growth the superficial area increases. Consequently, the current density and the overpotential peak decrease. In the sequence of the formation process, the potential of oxidation of the nickel hydroxide far away from the grid was reached. Oxygen evolution appears when oxidized material reaches the electrode surface getting in contact with the external solution. The potential stabilized in a new plateau when the evolution reaction of the oxygen had practically consumed whole current. In the formation process (Fig. 9), the first potential plateau for alpha/beta nickel hydroxide is 60 mV less anodic than beta nickel hydroxide. This assists the process of oxidation of the active material from alpha/beta nickel hydroxide. The second potential plateau, that is, the overload potential, is similar for both materials. Until the start of oxygen evolution, the detected charge (Q_F) was 80% of the theoretical charge (Q_T). This is calculated from the mass of the precursor material placed in the electrodes.

3.6.2. Active material morphology

During the formation process, there were volume changes in the $NiO{\cdot}OH/Ni(OH)_2$ positive electrodes. These changes provoked contraction and expansion movements in the electrodes. In the active material formation process, using the precursor material β-$Ni(OH)_2$, the unit cell volume decreased 15%, due to the transformation of β-$Ni(OH)_2$ in β-NiO·OH. In the overcharge β-NiO·OH became in γ-NiO·OH. In this case, there was a volume expansion of 44%

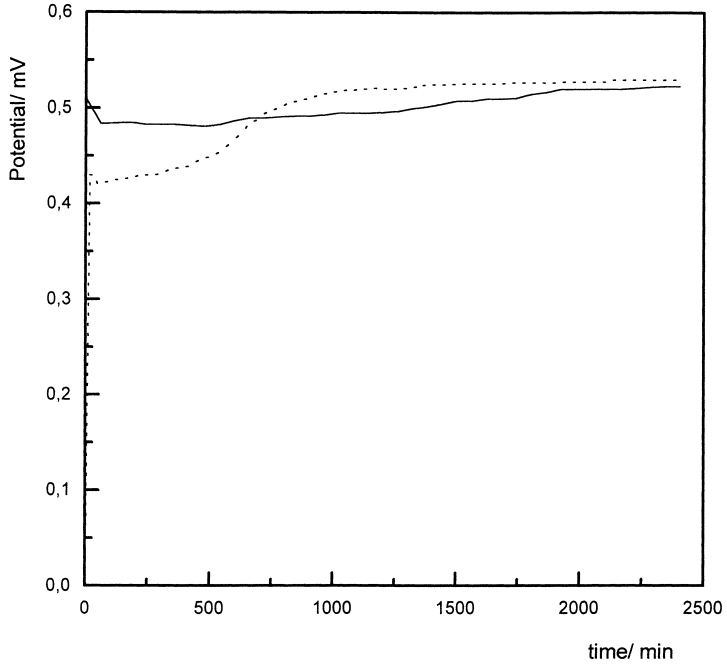

Fig. 9. Formation process: dotted line for alpha/beta nickel hydroxide and full line for beta-nickel hydroxide, formation current density (i_f) 23.0 mA/g (0.5 mA cm^{-2}).

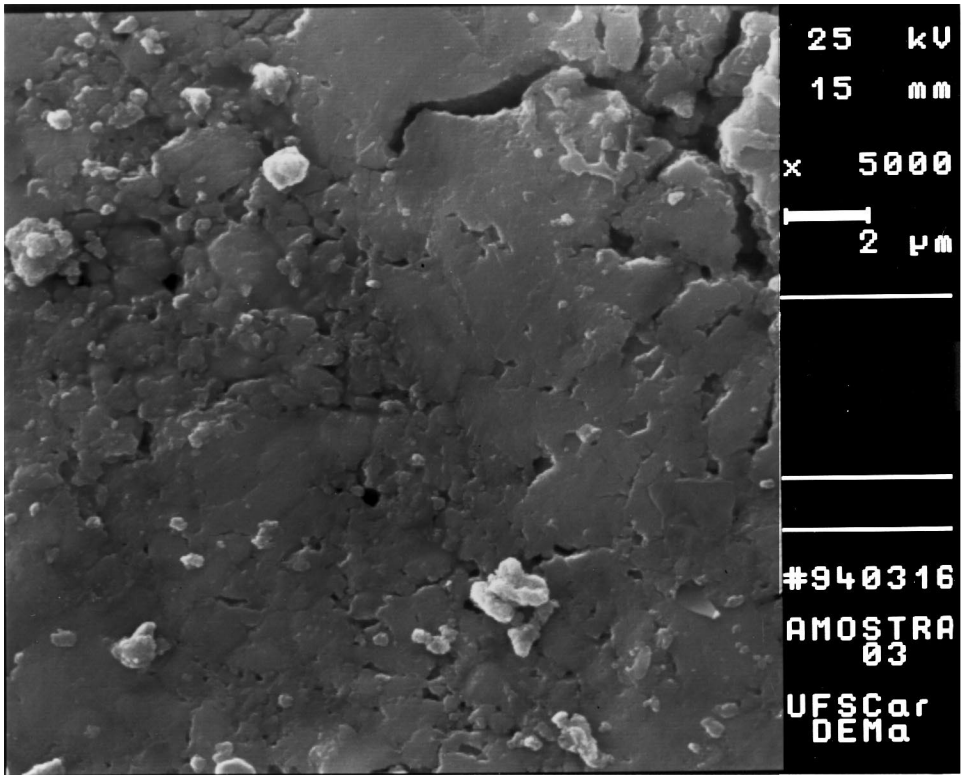

Fig. 10. SEM microphotograph of the electrode surface before formation process, beta nickel hydroxide as precursor material.

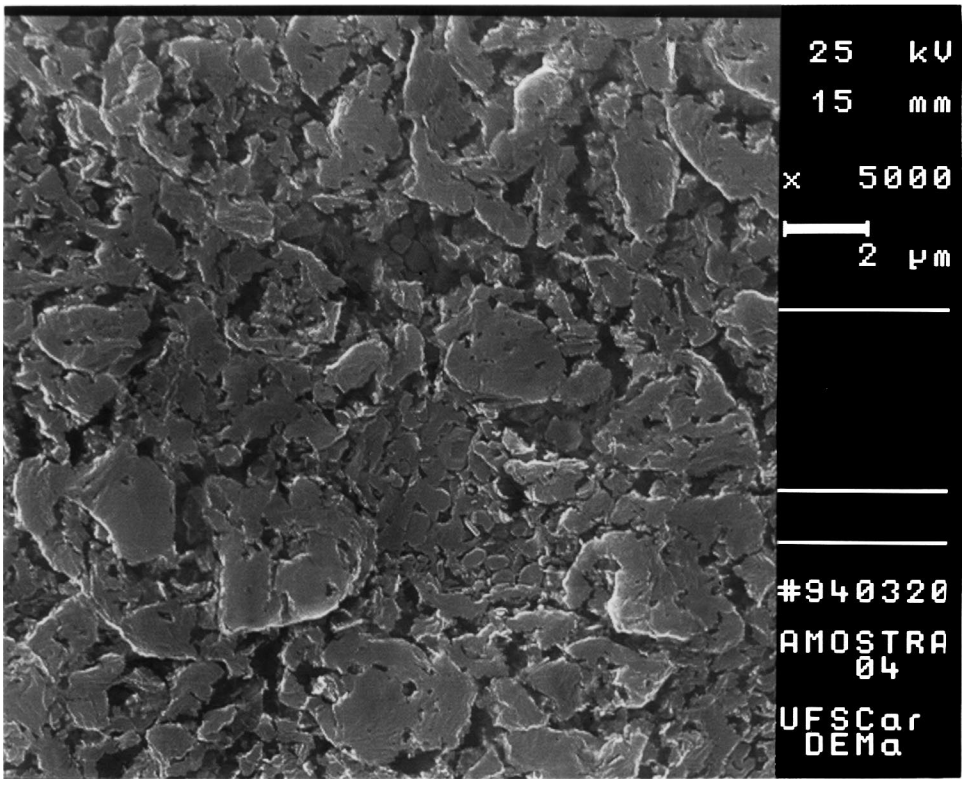

Fig. 11. SEM microphotograph of the electrode surface after formation process, beta nickel hydroxide as precursor material, current density (i_f) = 23.0 mA/g (0.5 mA cm^{-2}). The formation charge (Q_F) was 5.0 times the theoretical charge (Q_T).

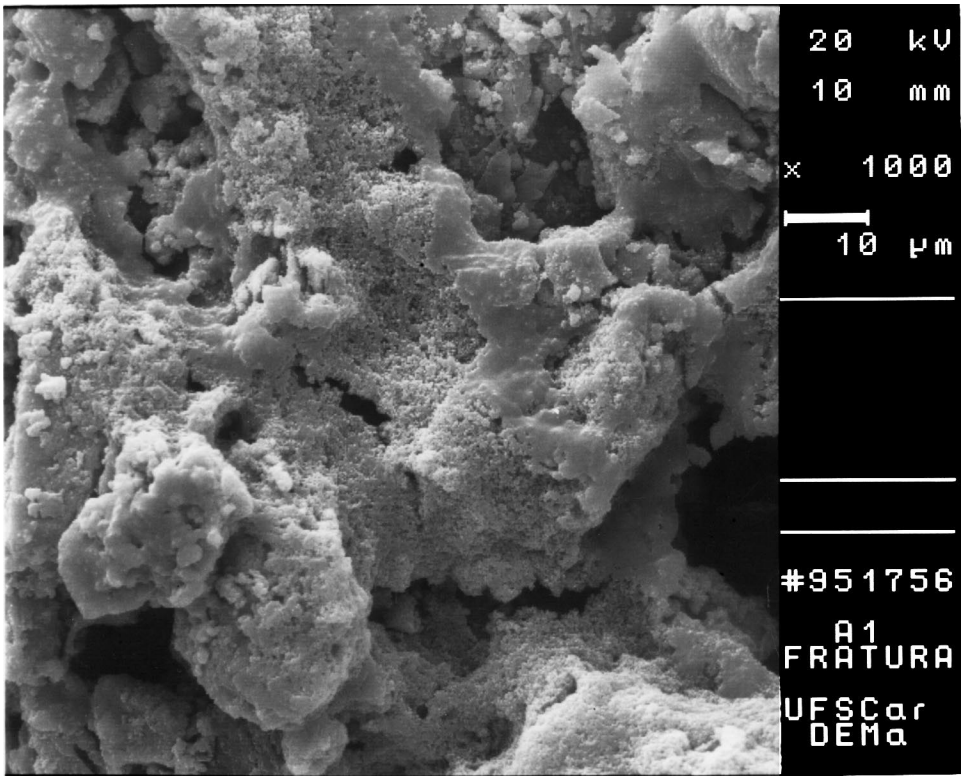

Fig. 12. SEM microphotograph of the active material inside of electrode, precursor material it was beta nickel hydroxide, formation current density (i_f) = 23.0 mA/g (0.5 mA cm^{-2}).

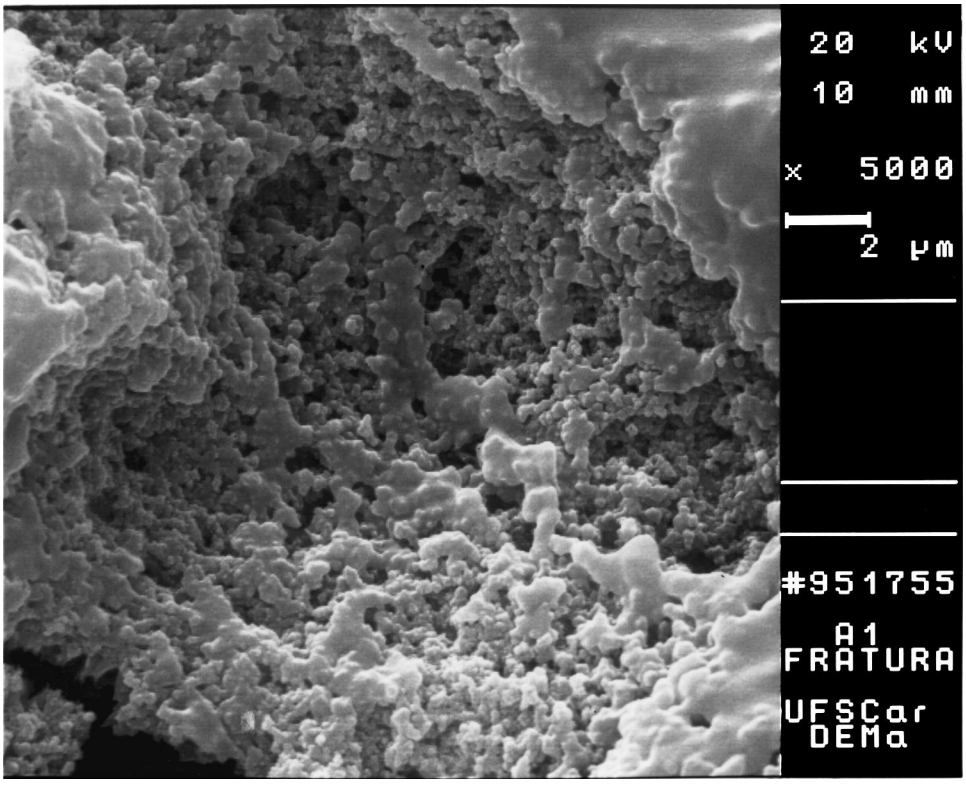

Fig. 13. Amplifications of the central area shown in the Fig. 12, current density (i_f) = 23.0 mA/g (0.5 mA cm^{-2}). The formation charge (Q_F) was 5.0 times the theoretical charge (Q_T).

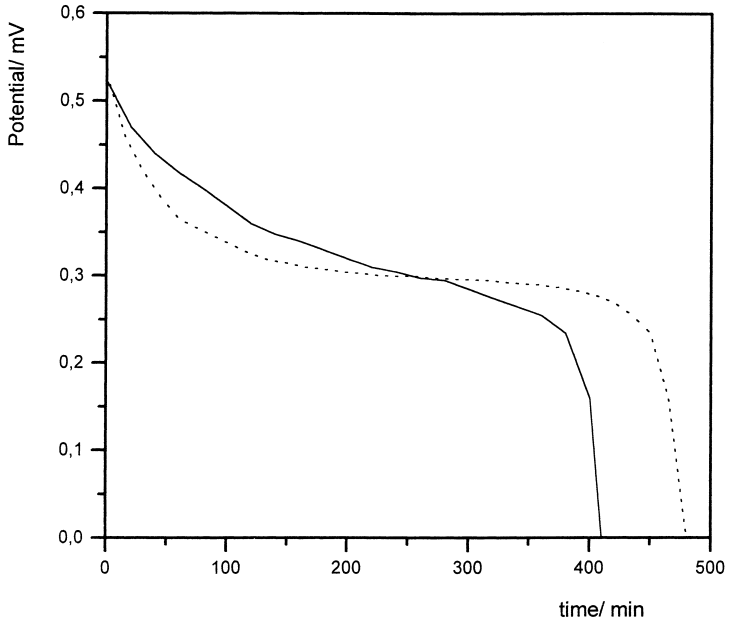

Fig. 14. Discharges plots for the active material synthesized from: dotted line for alpha/beta nickel hydroxide and full line for beta-nickel hydroxide, discharge current density (i_d) = 23.0 mA/g (0.5 mA cm^{-2}).

in the unit cell. When γ-NiO·OH was obtained from β-$Ni(OH)_2$, the oxidation process lead to a structural transformation that provoked molar volume variation and an increase in surface area. In the microphotographs shown in Figs. 10 and 11, this can be seen.

The microphotograph for active material inside the electrodes (Fig. 12) shows the macropores and micropores. These macropores will assure the diffusion of the solution to areas where the electrochemical reactions occur. Amplifications of the central parts of Fig. 12 are shown in the Fig. 13. In these microphotographs several micropores and very small particles having 0.5 μm size can be seen. These structures assure the connection in the active material and, at the same time, a great microporosity. Consequently, the electrodes have high specific capacity. The transformations involving α-$Ni(OH)_2$ in γ-NiO·OH does not cause significant volume change of the unit cell [5].

3.6.3. Active material discharge

The discharge curve shows constant potential drops with time (Fig. 14). This is less accentuated for γ-NiO·OH formed from alpha/beta nickel hydroxide as precursor material for the same current density. The discharge plot for γ-NiO·OH formed from alpha/beta nickel hydroxide as precursor material had a potential plateau around 0.3 V. This occurred due to the difference in the resistance of active material. As a consequence of its smaller resistance, the active material prepared form alpha/beta nickel hydroxide presented more capacity and mass utilization (Table 2). The resistance of active material increased during the discharge leading to a potential at higher cathodic values at current constant. When the amount of active material was used, an abrupt potential drop could be seen in the discharge plots.

Table 2
Electrodes discharges[a]

Precursor material	Resistance ($\Omega\ cm^{-2}$)	Capacity ($mAhg^{-1}$)	Mass utilization coefficient
α/β-$Ni(OH)_2$	147	180	61.5
β-$Ni(OH)_2$	253	156	53.3

[a] The average resistance of the electrodes was obtained dividing the linear potential drop in the discharge by current density.

4. Conclusions

In the material precursor synthesis, during the fast addition of reagent, many nuclei that did not have enough time to grow, were formed. As a result, the nickel hydroxide powder present a long specific superficial area. The nuclei coalesced forming big agglomerates composed of small nuclei. In the digestion stage, α-$Ni(OH)_2$ initially formed, was transformed into β-$Ni(OH)_2$ by an aging process, which means, by a dissolution and precipitation mechanism. Mixtures of β-$Ni(OH)_2$ and α-$Ni(OH)_2$ were produced after the aging process. The chemical compositions for alpha and beta nickel hydroxide are: $[\alpha/\beta\text{-}Ni(OH)_{2\text{-}K}(H_2O)_{0,65}(NO_3)_{2\text{-}U}(CO_3)_{2\text{-}W}]$, where 2-K, 2-U and 2-W are the amounts of OH^-, NO_3^- and CO_3^{2-}, respectively. For beta nickel hydroxide, the chemical composition is: $[\beta\text{-}Ni(OH)_{2-X}(H_2O)_{0,30}(SO_4)_{2-Y}(CO_3)_{2-Z}]$ where 2-X, 2-Y and 2-Z are the amounts of substances for OH^-, SO_4^{2-} and CO_3^{2-}, respectively. In the formation process, the oxidation potential for alpha/beta nickel hydroxide is 60 mV less anodic than beta nickel hydroxide. Therefore, it is easier for the preparation of the active material from alpha/beta nickel hydroxide oxidation. The discharge plot for γ-NiO·OH formed by oxidation

of the alpha/beta nickel hydroxide chemically synthesized, presented a smooth potential drop. Consequently, it has higher capacity, due to its lower resistance. Thus, new alpha/beta nickel hydroxide is a promising material for use in the positive electrodes of alkaline batteries as a substitution for β-$Ni(OH)_2$.

Acknowledgements

The author acknowledges CAPES for financial support for this research.

References

[1] J. McBreen, in: R.E. White, J.O'M. Bockris, B.E. Conway (Eds.), Modern Aspects of Electrochemistry, Vol. 21, Plenum Press, New York, 1990.
[2] P. Oliva, J. Leonard, J.F. Laurert, C. Delmas, J.J. Braconnier, M. Figlarz, F. Fievet, A. Guibert, J. Power Sources 8 (1982) 229.
[3] R.S. McEwen, J. Phys. Chem. 12 (1971) 1782.
[4] D. Tuomi, J. Electrochem. Soc. 112 (1965) 1.
[5] D. Singh, J. Electrochem. Soc. 145 (1998) 116.
[6] M.S. Kim, K.B. Kim, J. Electrochem. Soc. 142 (1998) 507.
[7] M.S. Kim, T.S. Hwang, K.B. Kim, J. Electrochem. Soc. 144 (1997) 1537.
[8] M.C. Bernard, P. Bernard, M. Keddam, S. Senyarich, H. Takenout, Electrochim. Acta 41 (1996) 91.
[9] M. Dixit, P.V. Kamath, V.G. Kumar, N. Munichandraiah, A.K. Shukla, J. Power Sources 63 (1996) 167.
[10] K. Micka, Z. Zabransky, J. Power Sources 8 (1982) 9.
[11] Joint Committee on Power Diffraction Standards (JCPDS), Card No. 22-0444.
[12] Joint Committee on Power Diffraction Standards (JCPDS), Card No. 14-0117.
[13] K. Nakamoto, Infrared and Raman Spectra of Inorganic and Coordination Compounds, Wiley, New York, 1986.
[14] F. Potemer, A. Delahaye-Vidal, M. Figlarz, J. Electrochem. Soc. 133 (3) (1992) 671.
[15] B. Mani, J.P. Neufville, J. Electrochem. Soc. 135 (1988) 800.